IUST
Iran University of Science and Technology

Iranian Journal of Electrical and Electronic Engineering

Journal Homepage: ijeee.iust.ac.ir

Performance Analysis of Disk Type Variable Reluctance Resolver under Mechanical and Electrical Faults

F. Tootoonchian*(C.A.) and F. Zare**

Abstract: Disk Type Variable Reluctance (DTVR) resolvers have distinguished performance under run out fault comparing to conventional sinusoidal rotor resolvers. However, their accuracy under inclined rotor fault along with different types of eccentricities includes static and dynamic eccentricities are questioned. Furthermore, due to thin copper wires that are used for signal and excitation coils of resolver there is high risk of short circuit fault in the coils. So, in this study the performance of the sinusoidal rotor DTVR resolver under the mentioned faults are studied. The quality of output voltages along with position error of the sensor is discussed. 3-D time stepping finite element method is used to show the effect of different faults. Finally, the prototype of the studied resolver is constructed and tested. The employed test bed is built in such a way that is able to apply controllable level of different mechanical faults. Good agreement is obtained between the finite element and the experimental results, validating the success of the presented analysis.

Keywords: Disk Type Variable Reluctance (DTVR) Resolver, Eccentricity, Resolver, Sinusoidal Variation of the Coupling Area, Short Circuit, 3-D Finite Element Analysis, Mechanical Faults.

1 Introduction

VARIABLE Reluctance (VR) resolvers are increasingly used in inverter-driven electric motor drives as position sensors. Like the measure of temperature, time, and pressure, the measure of position is an important aspect in science, engineering, and industry [1]. The common position sensors are optical encoders and resolvers. The traditional resolvers include a rotary winding and two stator windings located at right angle [2-6]. While, modern brushless resolvers mostly work based on sinusoidal variation of reluctance and have no winding on rotor. The VR resolvers are preferred to the encoders due to their ability to work in noisy, polluted environments with high variation of temperature and vibration [7-11]. Some other advantages of VR resolvers are the simple structure of rotor without any winding, frame-less design, and shorter axial length that makes them more convenient to be integrated into a motor, obtaining absolute position signals without increasing the manufacturing cost, and competitive price because of the introduction of software-based resolver-to-digital (R/D) conversion [12]. The traditional VR resolvers work based on the sinusoidal variation of air-gap length. So, their accuracy is significantly influenced by any unwanted change in the air-gap length. In the other word their accuracy under different types of eccentricities is questioned. It is shown in [13] that increasing the rotor saliency into more than 2-saliency leads to improve the accuracy of the fully-aligned resolver. However, 2-salincy variable air-gap length resolver has the best performance under eccentricities [12-14]. To solve this problem a new design is proposed in [7] for 2-salincy variable air-gap length resolver that is able to achieve the improved performance with high accuracy. Although the proposed resolver has outstanding performance in fully-aligned condition and under eccentricities, its accuracy is ruined under run-out error.

The next generation of VR resolvers work based on the sinusoidal variation of stator and rotor coupling area

Iranian Journal of Electrical & Electronic Engineering, 2018.
Paper first received 30 July 2017 and accepted 31 January 2018.
* The author is with the Electrical Engineering Department, Iran University of Science and Technology, Tehran, Iran.
E-mail: tootoonchian@iust.ac.ir.
** The author is with the Electrical Engineering Department, Isfahan University of Technology, Isfahan, Iran.
E-mail: f.zare.1373@gmail.com.
Corresponding Author: F. Tootoonchian.

[15,16]. These types of resolvers, so-called sinusoidal rotor resolvers, are less sensitive than variable air-gap ones against eccentricities [15,16]. However, under run out error their coupling area is changed and the accuracy of their detected position is ruined. So, in [8] a disk type configuration is proposed for the sinusoidal rotor resolver that has a robust performance under run out error. Then, in [17] some optimizations are done on the DTVR resolver to attain the minimum position error. The best position error in fully-aligned resolver is achieved by an 8-pole resolver with harmonic injected rotor. Although the performance of the DTVR resolvers with sinusoidal rotor under run out error is comprehensively discussed in [8], the effect of other mechanical faults includes static and dynamic eccentricities and inclined rotor types are not studied yet. Furthermore, since the used wires for signal and excitation coils are very thin (with the diameter of 60μm), it is very likely to happen turn-to-turn short circuit. So, in this paper the influence of eccentricities, inclined rotor and short circuit faults on the position error of the DTVR sinusoidal rotor resolver is investigated using 3-D time stepping finite element method. Finally, the finite element results are verified by experimental tests on the prototype resolver.

2 Structure of the DTVR Resolver

The studied DTVR resolver has a disk-shaped single stator/single rotor structure. As shown in Fig. 1(a), the stator has 16 radially grooved slots that contain a two phase concentrated windings (signal windings) and a peripheral slot in the middle of the core containing the excitation winding. The slots of the stator are skewed to reduce the spatial harmonics in the air-gap flux density distribution. It can be shown that to decrease slot harmonics, the skewing angle must be equal to one stator slot pitch [18]. Therefore, the skewing angle is considered equal to 22.5º for the studied resolver. As shown in Fig. 1(b) the rotor has a simple 8-pole structure without winding. To decrease third harmonic level in the output voltage's envelope of the studied resolver a calculated level of third harmonic is injected into the rotor contour [14], [17]. The assembled resolver is shown in Fig. 1(c). The geometrical dimensions and excitation parameters of the studied resolvers are presented in Table 1.

3 Principle of Operation

The studied resolvers work based on sinusoidal coupling area. Considering a sinusoidal excitation voltage as:

$$V_{ex} = V_m \cos(\omega t) \tag{1}$$

where V_m is the amplitude of the voltage, and ω is the angular frequency, the excitation current (I_{ex}) can be calculated as [8], [18,19]:

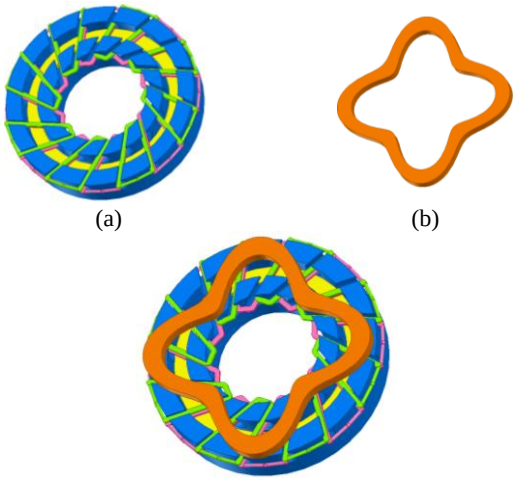

(a) (b) (c)

Fig. 1 The studied DTVR resolver, a) stator, b) 8-pole rotor and c) the assembled resolver.

Table 1 Geometrical Dimensions and Excitation Parameters of the DTVR Resolvers.

Parameter	Unit	Value
Excitation Voltage	V	5
Frequency	Hz	800
Pole pairs	-	4
Air gap length	mm	0.5
Skewing angle	Deg.	22.5
Core outer/inner diameter	mm	37.2/18.6
Stator/rotor axial length	mm	10/3
Number of stator slots	-	16
Slot width of stator	mm	2.5
Number of turns per phase of stator signal windings	-	100
Number of turns for excitation winding	-	70
Peripheral slot width	mm	3.33

$$I_{ex} = \frac{V_m}{\sqrt{R_{ex}^2 + L_{ex}^2 \omega^2}} \cos(\omega t - \arctan \frac{L_{ex}\omega}{R_{ex}}) \tag{2}$$

where R_{ex} and L_{ex} are the resistance and the inductance of the excitation winding, respectively. The excitation flux (ϕ_{ex}), can be calculated based on the multiplication of magneto motive force ($\Im_{ex}$) and the air-gap permeance (Λ):

$$\phi_{ex} = \Lambda \times \Im_{ex} = \mu_0 \frac{S}{\delta} \times \Im_{ex} = \mu_0 \frac{S}{\delta} \times N_{ex} I_{ex} \tag{3}$$

where δ is the length of the air gap, N_{ex} is the number of excitation coil turns, and S is the coupling area of the resolver and its value under the i^{th} stator tooth can be defined as:

$$S_i = K \cos\left(p\theta + (i-1)p \times \frac{2\pi}{Z_s} \right) \tag{4}$$

where K is defined based on geometrical parameters in [20] and p denotes pole pairs. Thus, the flux that passes

through the i^{th} stator tooth is:

$$\phi_i = \Lambda_i \times \Im_{ex,i} = \mu_0 \frac{K}{\delta} \cos\left(p\theta + (i-1) p \frac{2\pi}{Z_s} \right) \frac{\Im_{ex}}{Z_s} \quad (5)$$

Then, the flux linkage of the signal windings can be written as:

$$\psi_1 = \sum_{i=1,5,9,13} N_i \times \phi_i - \sum_{i=3,7,11,15} N_i \times \phi_i \quad (6)$$

$$\psi_2 = \sum_{i=2,6,10,14} N_i \times \phi_i - \sum_{i=4,8,12,16} N_i \times \phi_i \quad (7)$$

Substituting (5) into (6) and (7) and considering $N_i = N$ (the number of coil turns on each stator tooth), the flux linkages are calculated as:

$$\psi_1 = \frac{8N\mu_0 K}{Z_s \delta} N_{ex} I_{ex} \cos(p\theta) \quad (8)$$

$$\psi_2 = \frac{8N\mu_0 K}{Z_s \delta} N_{ex} I_{ex} \sin(p\theta) \quad (9)$$

Substituting (2) into (8) and (9), the flux linkages are recalculated as:

$$\psi_1 = \xi \cos(p\theta)\cos(\omega t - \sigma) \quad (10)$$

$$\psi_2 = \xi \sin(p\theta)\cos(\omega t - \sigma) \quad (11)$$

where

$$\xi = \frac{8N\mu_0 K}{Z_s \delta} \frac{N_{ex} V_m}{\sqrt{R_{ex}^2 + L_{ex}^2 \omega^2}} \quad (12)$$

$$\sigma = \arctan \frac{L_{ex}\omega}{R_{ex}} \quad (13)$$

Finally, the induced voltages can be written as:

$$V_1 = -\frac{d\psi_1}{dt} = \xi\omega \cos(p\theta)\sin(\omega t - \sigma) \quad (14)$$

$$V_2 = -\frac{d\psi_2}{dt} = \xi\omega \sin(p\theta)\sin(\omega t - \sigma) \quad (15)$$

Then, the angular position can be calculated as:

$$\theta = \frac{1}{p} \tan^{-1}\left(\frac{V_2}{V_1} \right) \quad (16)$$

4 Finite Element Analysis

Considering disk shape of the studied resolver, 3-D finite element analysis is required. Furthermore, to calculate the induced voltage, considering the high frequency excitation, the non-linear behavior of the core, and the effect of rotor's speed, non-linear time stepping transient method is needed. However, the accuracy of 3-D FEM is affected by three phenomena: magnetic core saturation, time step of solution and the quality of meshes. It is obvious by choosing smaller time steps and finer meshes the more accurate results are achieved. While, the solution time will also increase. In this study the total number of mesh elements is 45580 and the time step is chosen equal to 17.5μs. It is calculated in such a way that 2500 samples are available in one period of signal's envelope.

To ensure that the quality of signals is not affected by core saturation, the distribution of magnetic flux density on the studied health sensor is shown in Fig. 2(a). It can be seen the maximum flux density is less than 100mT while the magnetic flux density of the employed steel in its knee point is 0.25T. So, it can be sure the sensor is working in the linear part of the core's magnetization curve.

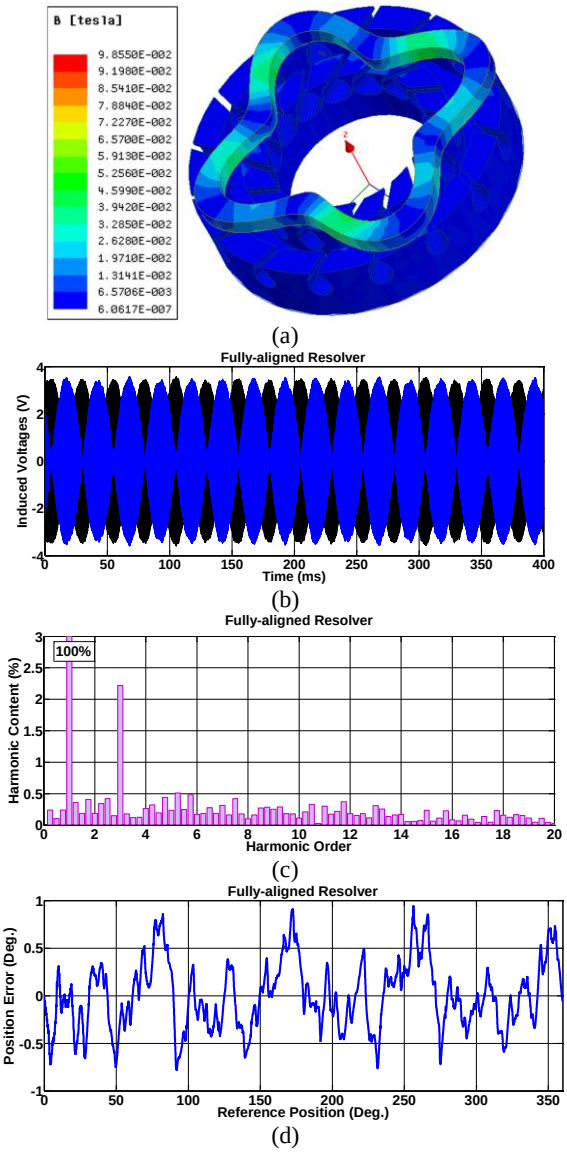

Fig. 2 The results of FEM in fully-aligned resolver: a) distribution of magnetic flux density at t = 0.425s, b) induced voltages, c) the harmonic content of voltages' envelope and d) the position error.

The induced voltages in the signal windings of the health sensor is presented in Fig. 2(b). As it can be seen although on-tooth winding is used for the stator, there is no obvious amplitude/quadrature error in the signals. It should be mentioned considering the on-tooth winding for the stator may lead to significant sub-harmonics with even higher amplitude than the main harmonics. So, it is important to measure the resolver signals in one mechanical revolution of the rotor and consider the effect of sub-harmonics. However, investigating the harmonic content of voltages' envelope in Fig. 2(c) shows the amplitude of sub-harmonics are almost neglected and the most significant harmonic is the third one. THD of voltages' envelope is 3.02%. The position error of the studied resolver is presented in Fig. 2(d). The maximum position error is 0.91º and the average of absolute position error is 0.30º.

It is predicted that occurring the faults will lead to increase the harmonic content of the voltages' envelope and the position error. So, in continue the performance of the sensor under different type of mechanical and electrical faults are discussed.

5 Performance under Fault Condition

As mentioned earlier, both mechanical and electrical faults are discussed. The studied mechanical faults are static and dynamic eccentricities and inclined rotor and the studied electrical faults consist of short circuit in excitation coil and short circuit in one or two signal windings.

5.1 Mechanical Faults

In fully-aligned resolver the symmetrical axis of stator, that of rotor and the rotational axis of rotor are coincide. However, when eccentricities occur the rotational axis of rotor is coinciding with the stator/rotor symmetrical axis while it is apart from the rotor/stator symmetrical axis. In cylindrical resolvers under static eccentricity (SE) where stator axis is apart from rotor and rotational axes the air-gap length in one side of air-gap is decreased and at the same time its length in the opposite side is increased. The location of minimum/maximum air-gap length is constant around the rotor. However, in disk type resolvers, under SE the air-gap length remains constant and only the coupling area between stator and rotor changes with respect to the fully-aligned resolver. So, disk type resolvers are less sensitive against SE than cylindrical ones. However, the studied disk type resolver works based on the sinusoidal variation of coupling area between the stator and rotor. So, it seems studying the performance of this sensor under SE is important. Three levels of SE are considered for simulations: 0.5, 1, and 2 mm. The amplitude of the first harmonic, THD of induced voltages' envelope, average of absolute position error and the maximum position error for the health resolver and the resolver under different levels of SE are presented in Figs. 3(a) through 3(d). As shown in Figs. 3(a) though 3(d), by increasing the SE level the amplitude of the first harmonic decreases while the average of absolute position error increases. The increment of both items for 0.5mm SE is slightly considerable. The maximum position error and the THD of induced voltages' envelope show a different pattern. The highest value of absolute position error is achieved for the resolver under 1mm SE.

Considering dynamic eccentricity (DE), the rotational axis of rotor is coinciding with the symmetrical axis of stator and they are apart from the symmetrical axis of rotor. In cylindrical resolvers under DE the location of minimum and maximum air-gap length changes with rotor's rotation. However, for disk type resolvers the air-gap length remains constant under DE. Three levels of DE are examined in this study: 0.5, 1, and 2 mm.

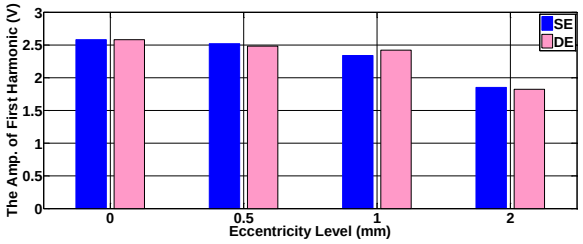

(a)

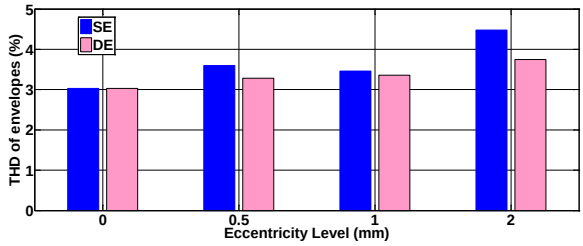

(b)

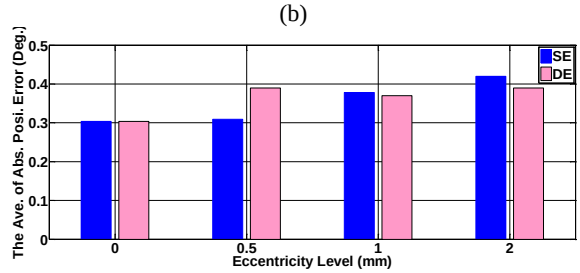

(c)

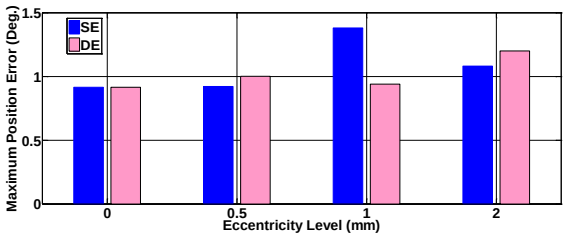

(d)

Fig. 3 The studied resolver under eccentricities: a) the amplitude of the first harmonic, b) THD of induced voltages' envelope, c) average of absolute position error and d) the maximum position error.

The amplitude of the first harmonic, THD of induced voltages' envelope, average of absolute position error and the maximum position error for the health resolver and the resolver under different levels of DE are also presented in Figs. 3(a) through 3(d). It can be seen that increasing the DE level leads to a reduction in the amplitude of the first harmonic while the THD of induced voltages' envelope, and the position errors shows an increase.

The highest increment of absolute position error under SE is 38.29% that is related to the 2mm SE. While, that value for the resolver under DE is about 28.4% that is related to both 0.5 and 2 mm DE. It should be mentioned although the amplitude of the first harmonic decreases under eccentricities, the reduction rate is not concerning. Furthermore, among the other characteristic factors (THD, average and maximum position error) the best one for judgment about the performance of a resolver is the average of absolute position error. Because, the value of THD is not sensitive to the harmonic order, phase shift error and quadrature error. Also, maximum position error is mostly due to the authors' employed technique (arc tangent method) for calculating position error.

Another mechanical fault that probably occurs is inclined rotor (IR) fault. Considering inclined rotor, the rotor is inclined around y-axis while its rotational axis is z-axis. So, the air-gap length is no more constant. The air-gap length is shortening in one side and in the opposite side it is enlarging. Three different rotation angles are examined in this study: 0.5°, 1°, and 1.5°.

The sine voltage's envelope versus that of cosine one in one mechanical rotation of rotor along with the THD of envelopes for different value of inclined rotor is shown in Fig. 4(a). It can be seen the amplitude of the voltages are decreased by increasing the inclination value. And the distortion of signals is increased with respect to the sinusoidal form. The maximum position error and the average of absolute position error for different level of inclined rotor faults are presented in Fig. 4(b). It can be seen the increment of position error under inclined rotor fault is more significant than that of eccentricities. The reason is related to the distortion in the air-gap length that is occurred under inclined rotor fault.

5.2 Electrical Faults

The electrical faults are divided into two groups: short circuit in excitation coil (SC-Exc.) and short circuit in signal windings (SC-Sig.). Five different scenarios are proposed for the second group of electrical faults:

1. short circuit in one of the sine/cosine coils (SC-Sig. 1);
2. short circuit in two sine/cosine coils under the same poles (SC-Sig. 2);
3. short circuit in two sine/cosine coils under two different poles (SC-Sig. 3);
4. short circuit in one sine and one cosine coils under the same poles (SC-Sig. 4);
5. short circuit in one sine and one cosine coils under two different poles (SC-Sig. 5).

Comparing the THD of induced voltage's envelope under different types of electrical errors in Fig. 5(a), indicates the most significant electrical fault is short circuit in the excitation coil. Among different scenarios of short circuit in signal windings the worst THD is related to SC-Sig. 2. The maximum and the average of absolute position error for different electrical faults are presented in Fig. 5(b). The highest value for the average of absolute position error belongs to SC-Sig. 2 that is related to the short circuit in two sine/cosine coils under the same poles. However, the worst maximum position error is related to SC-Sig. 3.

Finally, the performance of the studied resolver under electrical and the mechanical faults are summarized in Table 2. It can be seen, under both types of faults the position error and the THD of envelopes are increased with respect to the health resolver. However, the increment under different level of faults has no linear behavior.

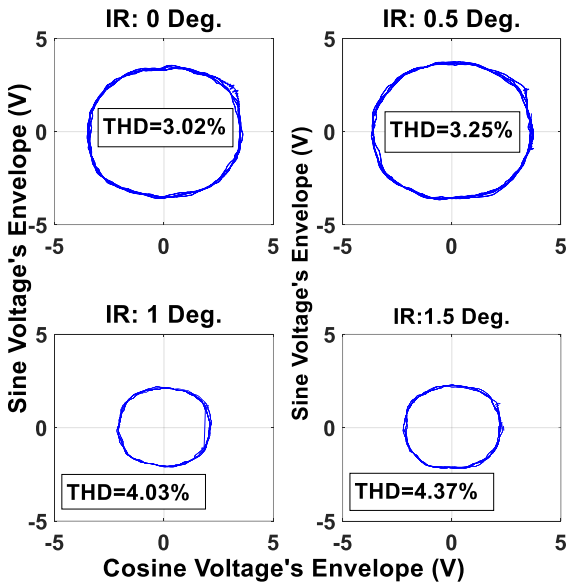

(a)

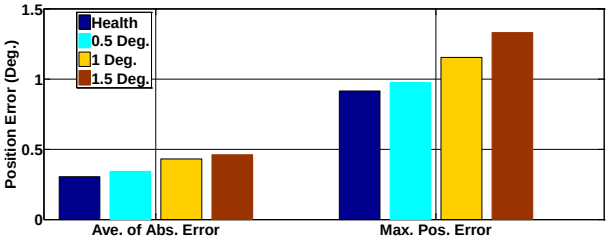

(b)

Fig. 4 The studied resolver under different level of inclined rotor fault: a) envelope of sine voltage versus that of cosine voltage for one mechanical rotation of rotor and b) the average of absolute position error and the maximum position error.

6 Experimental Validation

The prototype of the studied DTVR resolver is constructed. The stator along with the rotor are shown in Fig. 6(a). Fig. 6(b) shows the test circuit of the prototype. The test circuit is designed to be able to apply different types of mechanical faults include SE, DE, and IR. A rotary Tycope is used to measure and generate the rotational angle. To be sure that the resolver is coaxial with the Tycope, an adaptor with a Morse shaft (Conic shaft) has been constructed (Fig. 6(c)) and a depth micro-meter that is installed on an adaptor is used to displace the rotor with respect to the stator. The resolution of the employed micro-meter is 1μm. To apply different level of SE the stator must be displaced with respect to the rotor. The employed vertical clamp is used to move the stator with respect to the rotational axis of rotating plate. The level of

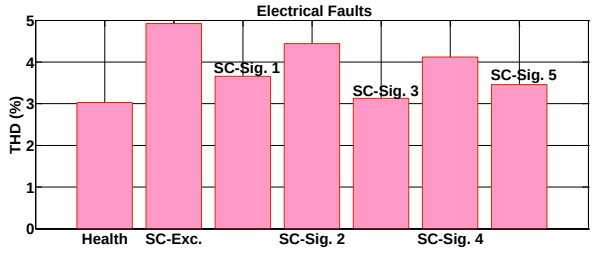

(a)

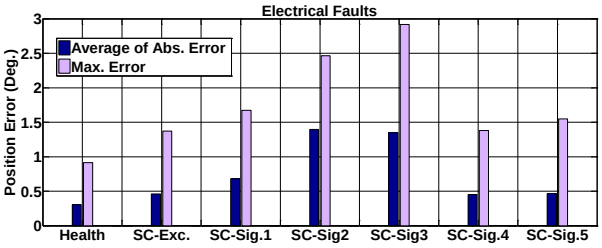

(b)

Fig. 5 The studied resolver under electrical faults: a) THD of induced voltage's envelope and b) average of absolute position error and the maximum position error.

Table 2 The performance of the studied resolver under different faults.

Fault type			THD (%)	Max. Pos. Error (Deg.)	Ave. of Abs. Error (Deg.)
Health resolver			3.02	0.91	0.30
Mechanical	SE	0.5 mm	3.60	0.92	0.31
		1 mm	3.46	1.38	0.38
		2mm	4.48	1.08	0.42
	DE	0.5 mm	3.28	1.00	0.39
		1 mm	3.36	0.94	0.37
		2mm	3.57	1.2	0.39
	IR	0.5º	3.25	0.97	0.34
		1º	4.03	1.15	0.43
		1.5º	4.37	1.33	0.46
Electrical	Exc.	SC-Exc.	4.65	1.39	0.43
	Sig.	SC-Sig.1	3.66	1.67	0.68
		SC-Sig.2	4.44	2.46	1.39
		SC-Sig.3	3.13	2.92	1.35
		SC-Sig.4	4.12	1.38	0.45
		SC-Sig.5	3.46	1.55	0.46

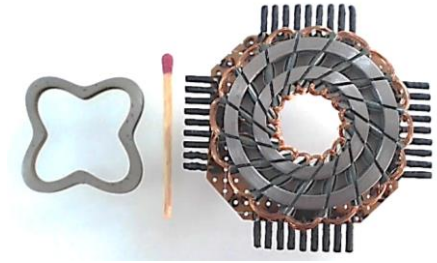

(a)

(b)

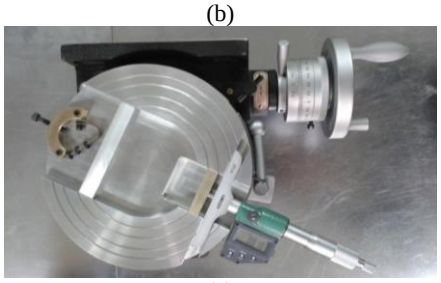

(c)

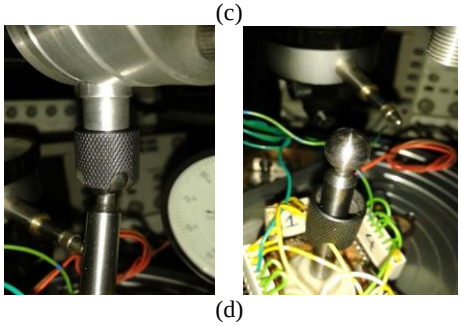

(d)

Fig. 6 The experimental evaluation: a) the stator, and the rotor, b) the test circuit, c) the adaptor with a Morse shaft (Conic shaft) and d) the employed ball joint for connection between the vertical clamp and the stator.

movement is measured using the employed indicators. In the inclined rotor fault, the surface of stator is inclined with respect to the rotor.

As shown in Fig. 6(d) in the designed test circuit the connection between the vertical clamp and the stator is established using a ball joint. So, different levels of inclined rotor fault are adjustable.

Besides the mechanical faults, the electrical faults were studied using FEM. To experimentally validate the simulation results, short circuit fault in excitation coil and the worst case of short circuit fault in signal windings (SC-Sig.2) are evaluated experimentally. In practice a desirable part of coil is selected and shorted by soldering. Then the soldered part is insulated by air-dry varnish. The producer is presented in Fig. 7. In all tests the excitation coil is supplied using a digitally synthesized function generator with the resolution of 0.1Hz and the amplitude of excitation voltage is adjusted using an automatic gain control circuit. Analogue voltages are saved and captured using a digital oscilloscope with the sampling rate of 1 GS/sec.

Finally, Hilbert transformation is used to calculate envelop of signals and then the angular position is calculated based on the arctangent of envelopes ratio. The calculated position is compared with the reference position (that of Tycope) to obtain the position error.

The analog output voltages for the healthy resolver is presented in Fig. 8(a). Those for the resolver under 2 mm SE, 2 mm DE, 1.5˚ IR is presented in Figs. 8(b) through 8(d). The analogue voltages under electrical faults are presented in Fig. 9(a), and 9(b). The measured analogue voltages are used to calculate the position error of the sensor. Fig. 10 shows the average of absolute position error calculated based on experimentally measured voltages and the results of finite element analysis. It can be seen that the error between simulation and experimental results is less than 5% that validates the presented discussions.

7 Conclusion

In this paper, the effect of different mechanical and electrical faults on the accuracy of a disk type variable reluctance resolver was discussed. The studied disk type resolver worked based on sinusoidal variation of coupling area between the stator and the rotor and it was less sensitive against run out fault. However, its performance under different types of eccentricities and inclined rotor faults was not investigated previously. It was shown the studied resolver had pride performance under eccentricities with respect to conventional cylindrical resolvers due to keeping the air-gap length constant. Furthermore, electrical faults are also probable in resolvers due to thin employed wires. So, short circuit fault in excitation coil and the signal windings was also studied. Five different scenarios were presented for short circuit fault in signal windings. It was shown that the highest value for average of absolute position error

Fig. 7 The practical representation of short circuit in coils.

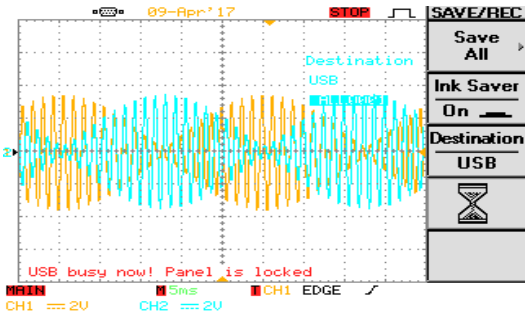

(a)

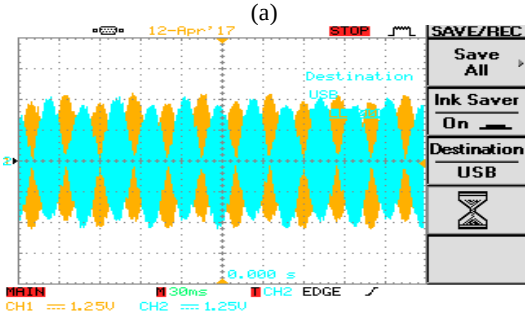

(b)

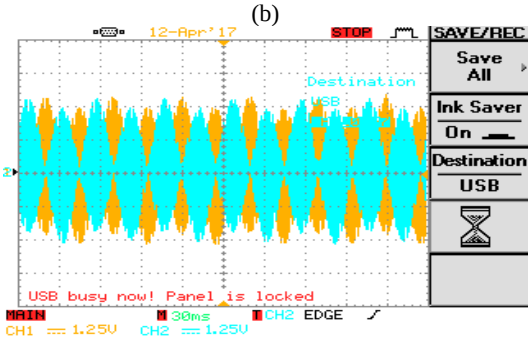

(c)

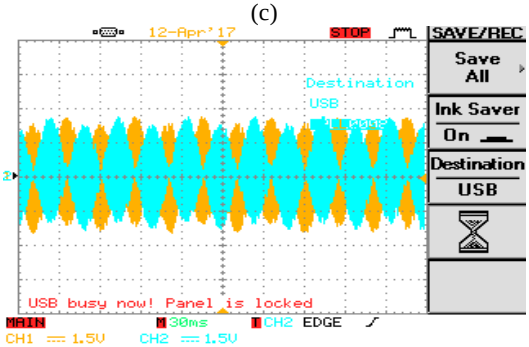

(d)

Fig. 8 The measured analogue voltages: a) Healthy resolver, b) under 2mm SE, c) under 2mm DE and d) under 1.5° inclined rotor.

is related to the short circuit in two sine/cosine coils under the same poles. All the simulations were carried out using 3-D time stepping finite element method. Finally, experimental tests on the prototype sensor were employed to validate the simulations.

Acknowledgment

This research has been done in continue of a B.Sc. project in the Sharif University of Technology and the authors would like to appreciate all the supports.

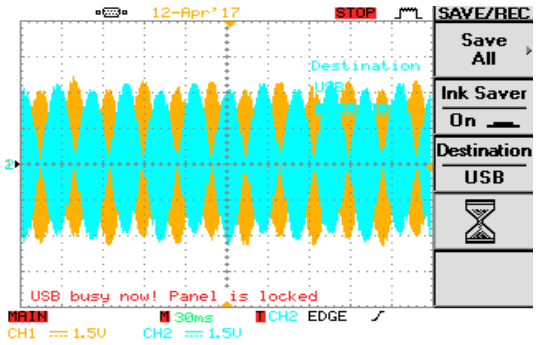

Fig. 9 The measured analogue voltages under electrical faults: a) under short circuit in excitation coil and b) under short circuit in signal winding considering SC-Sig. 2 fault condition.

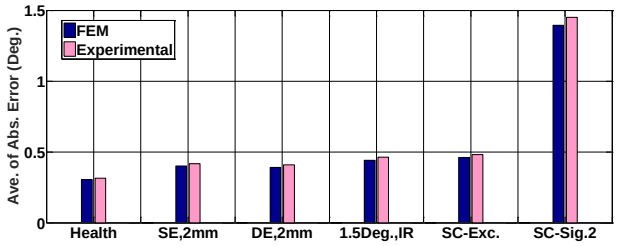

Fig. 10 Measured average of absolute position error in comparison with FEM results under different fault scenarios.

References

[1] A. Daniar, Z. Nasiri-Gheidari, and F. Tootoonchian, "Position Error Calculation of Linear Resolver under Mechanical Fault Conditions," *IET Science, Measurement & Technology*, Vol. 11, No. 7, pp. 948–954, 2017.

[2] M. Benammar, and A. S. P. Gonzales, "A Novel PLL Resolver Angle Position Indicator," *IEEE Transactions on Instrumentation and Measurement*, Vol. 65, No. 1, pp. 123–131, Jan. 2016.

[3] Z. Nasiri-Gheidari, and F. Tootoonchian, "Axial flux resolver design techniques for minimizing position error due to static eccentricities," *IEEE Sensors Journal*, Vol. 15, No. 7, pp. 4027–4034, Jul. 2015.

[4] Z. Nasiri-Gheidari, "Design, Analysis, and Prototyping of a New Wound-Rotor Axial Flux Brushless Resolver," *IEEE Transactions on Energy Conversion*, Vol. 32, No. 1, pp. 276–283, 2017.

[5] R. Alipour-Sarabi, Z. Nasiri-Gheidari, F. Tootoonchian, and H. Oraee, "Effects of Physical Parameters on the Accuracy of Axial Flux Resolvers," *IEEE Transactions on Magnetics*, Vol. 53, No. 4, pp. 1–11, Apr. 2017.

[6] R. Alipour-Sarabi, Z. Nasiri-Gheidari, F. Tootoonchian, and H. Oraee, "Analysis of Winding Configurations and Slot-Pole Combinations in Fractional-Slots Resolvers," *IEEE Sensors Journal*, Vol. 17, No. 14, pp. 4420–4428, Jul. 2017.

[7] F. Tootoonchian, and Z. Nasiri-Gheidari, "Twelve-slot Two-Saliency Variable Reluctance Resolver with Nonoverlapping Signal Windings and Axial Flux Excitation," *IET Electric Power Applications*, Vol. 11, No. 1, pp. 49–62, 2017.

[8] Z. Nasiri-Gheidar, F. Tootoonchian, and F. Zare, "Design Oriented Technique for Mitigating Position Error Due to Shaft Run-out in Sinusoidal-Rotor Variable Reluctance Resolvers," *IET Electric Power Applications*, Vol. 11, No. 1, pp. 132–141, 2017.

[9] F. Tootoonchian, "Design, Performance, and Testing of a Brushless Axial Flux Resolver Without Rotor Windings," *IEEE Sensors Journal*, Vol. 16, No. 20, pp. 7464–7471, 2016.

[10] Z. Nasiri-Gheidari, and F. Tootoonchian, "The Influence of Mechanical Faults on the Position Error of an Axial Flux Brushless Resolver without Rotor Windings," *IET Electric Power Applications*, Vol. 11, No. 4, pp. 613–621, 2017.

[11] H. Saneie, Z. Nasiri-Gheidari, and F. Tootoonchian, "Design-Oriented Modeling of Axial-flux Variable-reluctance Resolver Based on Magnetic Equivalent Circuits and Schwarz–Christoffel Mapping," *IEEE Transactions on Industrial Electronic*, early access.

[12] X. Ge, Z. Q. Zhu, R. Ren, and J. T. Chen, "A Novel variable reluctance resolver for HEV/EV applications," *IEEE Transactions on Industrial Applications*, Vol. 52, No. 4, pp. 2872–2880, Jul.–Aug. 2016.

[13] X. Ge, Z. Q. Zhu, R. Ren, and J. T. Chen, "A novel variable reluctance resolver with nonoverlapping tooth-coil windings," *IEEE Transactions on Energy Conversation*, Vol. 30, No. 2, pp. 784–794, May 2015.

[14] X. Ge, and Z. Q. Zhu, "A novel design of rotor contour for variable reluctance resolver by injecting auxiliary air-gap permeance harmonics," *IEEE Transactions on Energy Conversion*, Vol. 31, No. 1, pp. 345–353, Mar. 2016

[15] J. Shang, H. Wang, M. Chen, N. Cong, Y. Li, and C. Liu, "The Effects of Stator and Rotor Eccentricities on Measurement Accuracy of Axial Flux Variable-reluctance Resolver with Sinusoidal Rotor," *17th International Conference on Electrical Machines and Systems (ICEMS)*, Hangzhou, China, pp. 1206–1209, Oct. 2014.

[16] S. Jing, W. Hao, and W. Weiqiang, "The Analysis of Multi pole Axial Flux Reluctance Resolver with Sinusoidal Rotor," in *Proc. ECCE*, Harbin, China, pp. 1206–1209, 2012.

[17] Z. Nasiri-Gheidari, R. Alipour-Sarabi, F. Tootoonchian, and F. Zare, "Performance Evaluation of Disk Type Variable Reluctance Resolvers," *IEEE Sensors Journal*, Vol. 17, No. 13, pp. 4037–4045, Jul. 2017.

[18] Z. Nasiri-Gheidari, "Design, Performance Analysis, and Prototyping of Linear Resolvers," *IEEE Transactions on Energy Conversion*, Vol. 32, No. 4, pp. 1–10, Dec. 2017.

[19] H. Saneie, Z. Nasiri-Gheidari, and F. Tootoonchian, "An Analytical Model for Performance Prediction of Linear Resolver," *IET Electric Power Applications*, Vol. 11, No. 8, pp. 1457–1465, Sep. 2017.

[20] S. Jing, L. Chengjun, and Z. Jibin, "The Analysis for New Axial Variable Reluctance Resolver with Air-gap Complementary Structure," in *International Conference on Electrical Machines and Systems (ICEMS)*, Tokyo, Japan, pp. 1–6, Nov. 2009.

F. Tootoonchian received the B.Sc. and M.Sc. degrees in Electrical Engineering from the Iran University of Sciences and Technology, Tehran, Iran, in 2000 and 2007, respectively, and the Ph.D. degree from the K. N. Toosi University of Technology, Tehran, in 2012. He is currently an Assistant Professor with the Department of Electrical Engineering, Iran University of Sciences and Technology. His research interests include design, optimization, finite-element analysis, and prototyping of ultrahigh-speed electrical machines and ultrahigh-precision electromagnetic sensors.

F. Zare received the B.Sc. degree in Electrical Engineering from the Sharif University of Technology, Tehran, Iran, in 2016. She is currently M.Sc. student in Isfahan University of Technology. Her research interests include design and optimization of electrical machines and electromagnetic sensors.